REVISTA MEXICANA DE CIENCIAS GEOLÓGICAS

Revista Mexicana de Ciencias Geológicas, v. 43, num. 2, August 2026, 88–101
ISSN-L 2007-2902
https://rmcg.unam.mx

Type: Original research

DIAMOND OPEN ACCESS

Determination of the effective storage of CO_2 at Coyula seismic block level in the Tampico-Misantla province

Erik Medina[1, a], Gilles Levresse[2, b,*], Cesar A. Cortes-Prado[1, c], Mariano Cerca[2, d], Jaime Carrera-Hernandez[2, e], and Berengere Mougel[2, f]

[1] *Posgrado en Ciencias de la Tierra, Universidad Nacional Autónoma de México, UNAM Campus Juriquilla Blvd. Juriquilla 3001, Querétaro, 76230, Mexico.*
[2] *Instituto de Geociencias, Universidad Nacional Autónoma de México, UNAM Campus Juriquilla Blvd. Juriquilla 3001, Querétaro 76230, Mexico.*

**Corresponding author (G. Levresse): glevresse@geociencias.unam.mx*
[a] *0000-0002-8703-2747;* [b] *0000-0001-9290-9825;* [c] *0000-0002-7916-5398;* [d] *0000-0002-9264-4553;* [e] *0000-0002-4418-9277;* [f] *0000-0002-9226-7700*

Editors:
Luca Ferrari
Luigi A. Solari

How to cite:
Medina, E., Levresse, G., Cortes-Prado, C. A., Cerca, M., Carrera-Hernandez, J., & Mougel, B. (2026). Determination of the effective storage of CO_2 at Coyula seismic block level in the Tampico-Misantla province, *43*(2), 88–101. DOI: https://dx.doi.org/10.22201/igc.20072902e.2026.2.1900

Manuscript received: August 6, 2025
Corrected manuscript received: March 31, 2026
Manuscript accepted: April 6, 2026
Published online: August 1, 2026

Copyright
© 2026 The Author(s).
This is an open-access article published and distributed by the Universidad Nacional Autónoma de México under the terms of a Creative Commons Attribution 4.0 International License (CC BY) which permits unrestricted use, distribution, and reproduction in any medium, provided the original author and source are credited.

ABSTRACT

Carbon capture and storage methods are commonly accepted as an essencial way to mitigate atmospheric CO_2 concentrations. Despite being a significant petroleum producer, Mexico is committed to combating climate change encouraging the use of carbon capture and storage and enhance oil recovery technology. In this research, the storage capacity of CO_2 in the reservoir of a deep saline aquifer located in the Coyula seismic block in the Tampico Misantla Basin, is estimated using the volumetric approach where parameters like CO_2 density, and porosity of the geological formation, and efficiency storage factor are considered. To achieve a better evaluation of the site and to constrain the effective storage potential of the Coyula seismic block, both open and close systems were tested. A conservative evaluation for all the identified reservoirs, delimited in the Cahuasas Jurassic formation within the Coyula seismic block, amounts to 25.6 Mton CO_2. Compared to the emissions from regional sources (8 Mton of CO_2 per year), the minimum geological reservoir evaluation encourages further detailed studies to improve the estimation of reservoir volumes and CO_2 storage feasibility.

Keywords: Screening and evaluation of CO_2 storage; saline aquifer; CO_2 storage; regional characterization; Mexico

RESUMEN

Los métodos de captura y almacenamiento de carbono son ampliamente aceptados como una forma esencial de mitigación de las concentraciones atmosféricas de CO_2. A pesar de ser un importante productor de petróleo, México está comprometido con la lucha contra el cambio climático, promoviendo el uso de tecnologías de captura y almacenamiento de carbono, así como de recuperación mejorada de petróleo. En esta investigación, se estima la capacidad de almacenamiento de CO_2 en el reservorio de un acuífero salino profundo ubicado en el bloque sísmico Coyula, en la Cuenca Tampico-Misantla, utilizando el enfoque volumétrico, en el cual se consideran parámetros como la densidad del CO_2, la porosidad de la formación geológica y el factor de eficiencia de almacenamiento. Para lograr una

DOI: https://dx.doi.org/10.22201/igc.20072902e.2026.2.1900

mejor evaluación del sitio y delimitar el potencial efectivo de almacenamiento del bloque sísmico Coyula, se analizaron tanto sistemas abiertos como cerrados. Una evaluación conservadora de todos los reservorios identificados, delimitados en la formación jurásica Cahuasas dentro del bloque sísmico Coyula, arroja una capacidad de almacenamiento de 25.6 millones de toneladas de CO_2. En comparación con las emisiones de las fuentes regionales (8 millones de toneladas de CO_2 por año), la evaluación mínima del reservorio geológico fomenta la realización de estudios más detallados para mejorar la estimación de los volúmenes del reservorio y la viabilidad del almacenamiento de CO_2.

Palabras clave: *selección y evaluación del almacenamiento de CO_2; acuífero salino; almacenamiento de CO_2; caracterización regional; México*

INTRODUCTION

The increasing concentration of CO_2 in the atmosphere due to the development of industrial activity during the last century has significantly impacted the global climate, the ecological environment and is currently jeopardizing our way of life. Concerned for the consequences of carbon concentrations, societies have called for a global effort to limit the CO_2 emissions or to reverse the increasing trend of CO_2 concentration in our atmosphere. To reduce the amount of CO_2 in the atmosphere, Carbon Capture and Storage (CCS) methodologies have been recommended as a viable option (Torp and Gale, 2003).

Accordingly, CCS methods have been continuously developed since the 1990s. One of the most promising approaches is CO_2 storage in saline aquifers, because it offers a high-potential carbon storage under CO_2 supercritical conditions (31.1 °C and 7.38 MPa), and CO_2 can be retained at depth through several processes, such as structural/stratigraphic trapping, residual trapping (capillarity force in porosity at irreducible gas saturation), solubility trapping (dissolved into formation water), as well as mineral trapping (incorporated in newly formed minerals during water/rock interaction). As any geological injection processes, injection of CO_2 into deep saline aquifers is not an easy task. It requires a multicomponent, multiphase flow system, in which geomechanics, geochemistry, and thermal effects may be important (Al-Khoury and Bundschuh, 2014).

The capacity of CO_2 storage in geological formation is not consequently a straightforward or simple process. Luo *et al.* (2022) have recently reviewed the different storage mechanism applied worldwide and pointed out the challenges of evaluating the different stages involved. The CO_2 storage capacity estimation methods are divided in static and dynamic methodologies. Static methods involve the characterization of the physical properties of the aquifer, such as porosity and permeability, to calculate the total volume. The dynamic methods involve simulating the fluid flow and transport processes in the aquifer to estimate the effective storage potential, and the CO_2 behavior over the time (Bachu, 2003). The dynamic methods require defining more data to characterize the thermal mechanic and hydrologic processes. It also requires more precise boundary conditions of the potential reservoir rock and fluids. In close systems, the reservoir volume is restricted by the impermeable geological boundary (structural or stratigraphic), which prevent fluid movement, and volume variation. Conversely, open systems permit vertical and/or lateral fluid movements through permeable boundaries, thereby increasing porosity availability and enabling volume variations.

This study evaluates the CO_2 storage potential of Jurassic saline aquifers in the Tampico-Misantla Basin, focusing on Coyula seismic block scale as a last step before dynamic, site-specific evaluations. The main objective is to estimate effective storage capacity using locally derived petrophysical data, aiming to reduce uncertainty associated with global averages commonly used in previous studies, such as those by the IEA-GHG (2009). A lithostratigraphic-structural model was developed, identifying three potential storage sites within the basin. Static storage capacity was calculated using effective storage coefficients tailored to local geological conditions. This approach addresses challenges related to limited site-specific data, which currently prevent detailed dynamic modeling of CO_2 flow and transport. The study builds on prior regional assessments that highlighted the suitability of the basin for carbon capture and storage, offering refined estimates that can support future CCS planning and implementation in northeastern Mexico.

GEOLOGICAL FRAMEWORK

The central part of the Mexican continental margin of the Gulf of Mexico is composed of the Tampico Misantla basin (TMB; Figure 1) which consists of a low-lying (0 to 500 m a.s.l) mountainous plain. Its northern part is bordered by the Sierra de Tamaulipas, and to the south is the Trans Mexican Volcanic Belt. On the western and eastern sides, the TMB is bounded by the Gulf of Mexico, and the Sierra Madre Oriental, respectively.

The Sierra Madre Oriental belongs to the Mexican Fold and Thrust Belt tectonic unit (MFTB; Figure 1; Fitz-Díaz *et al.*, 2018). Its formation is related to the Laramide Orogeny and the associated subsidence of former carbonate platforms together with the development of Late Cretaceous–Paleogene flexural Mexican Foreland Basins (MFB, Figure 1; Suter, 1980; Roure *et al.*, 2009; Lawton *et al.*, 2016) including the Burgos (BB), the Tampico-Misantla (TMB), and the Veracruz Basin (VB). The MFB forms a large and low-altitude terrain in direct contact with the MFTB (Eguiluz de Antuñano, 2011). Overall, the TMB itself exhibits a complex geological record, where Mesozoic sediments overlie the Precambrian and Paleozoic basement, which in turn underlies Triassic units of volcanic and sedimentary origin (Carrillo-Bravo, 1971; Fitz-Díaz *et al.*, 2018).

Figure 1 presents a geological map detailing the lithology of geological units from the region, as well as and the main structures which show evidence for tectonic shortening and extension. The sedimentary and structural contacts between units from the Jurassic to more recent periods are illustrated in a redrawn regional geological cross-section from the Comisión Nacional de Hidrocarburos (2018; A-A' profile in Figure 1). It is worth pointing out that the study area has been affected by the pre- and syn- rifting and drifting episodes of the Gulf of Mexico (GOM) during the Jurassic, which led to the reworking of the continental rocks and syn-rift sediments formed before the Jurassic (Coombs *et al.*, 2020). The subsequent rotational opening of the GOM coupled with the translation of the Yucatan Block enabled the

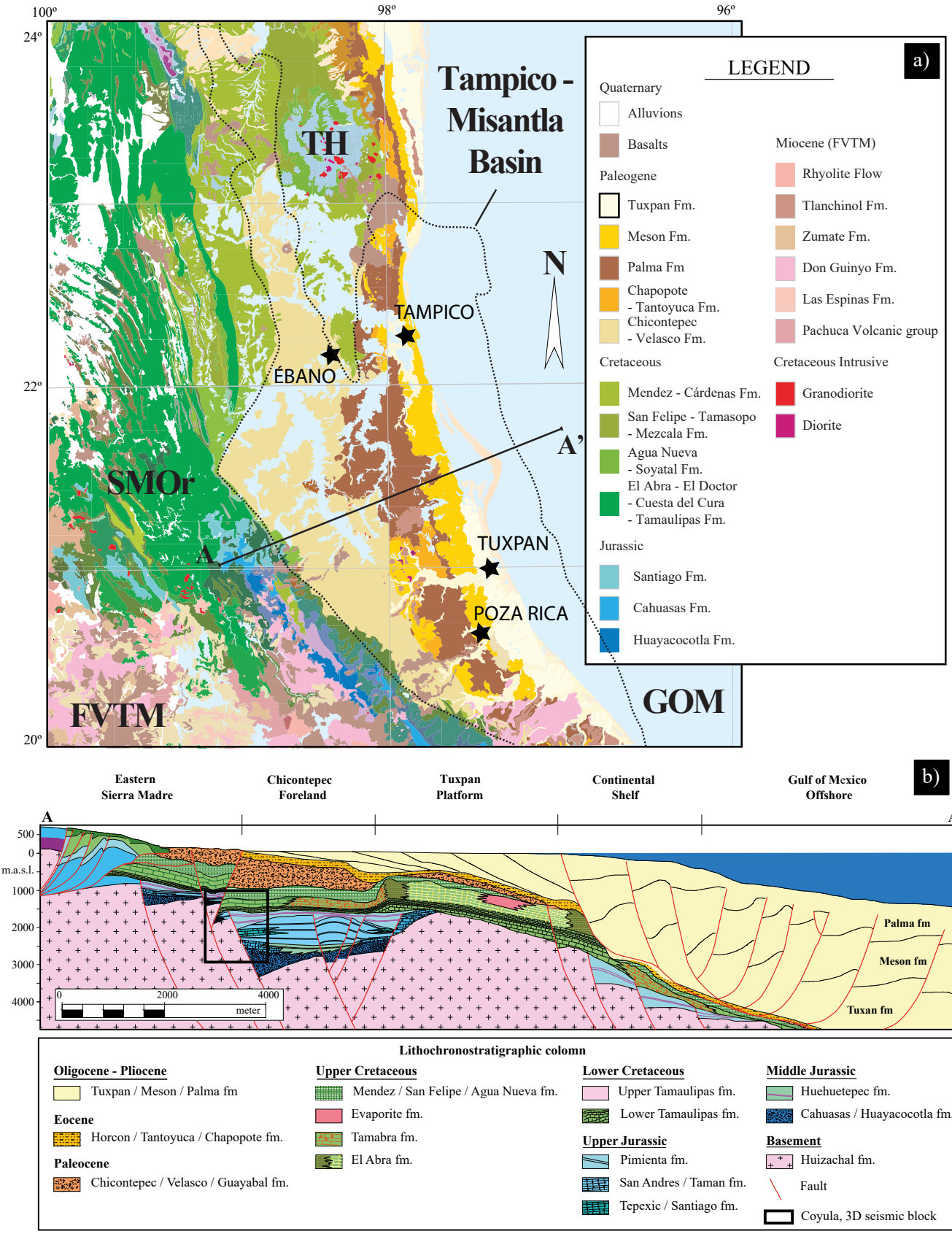


Figure 1. a) Geologic map of the Tampico Misantla Basin (TMB; modified from Servicio Geologico Mexicano (1997a; 1997b; 1999; 2002; 2004a; 2004b; 2004c; 2004d). b) E-W Geologic section A- A' of the Tampico Misantla Basin (modified from Comision Nacional de Hidrocarburos (2018). GOM: Gulf of Mexico. FVTM: Faja Volcanica Trans Mexicana; SMOr: Sierra Madre Oriental; TH: Tamaulipas Highs. The black square represents the Coyula seismic block. Black star: main cities.

RMCG | v. 43 | núm. 2 | www.rmcg.unam.mx | DOI: https://dx.doi.org/10.22201/igc.20072902e.2026.2.1900

formation of north-south regional shear zones across eastern Mexico (Pindell *et al.*, 2020; Coombs *et al.*, 2020). These zones accommodated substantial displacements, fragmenting paleogeographic elements like the massif of Chiapas and that of Tampico (Pindell *et al.*, 2020; Coombs *et al.*, 2020) and ultimately followed by the development of the extensional TMB (Martini and Ortega, 2018). Reported evidence for post-rift facies and carbonate platform deposition (Hernández-Romano *et al.*, 1997) suggest that a passive margin environment was prevailing throughout much of the Cretaceous. However, during the Paleocene-Eocene, the deformation characterized by significant shortening led to the formation of the Chicontepec foreland sub-Basin, being related to the Mexican Orogenic event (Fitz-Díaz e*t al.*, 2018). This basin is composed of siliciclastic sediments deposited during the orogenic period (Eguiluz de Antuñano, 2011; Fitz-Díaz *et al.*, 2018). Consequently, formations formed prior and during the Mesozoic experienced deformation and structuring within the fold-thrust belt, with the migration of the shortening front towards the east and overriding units of Middle Cretaceous age onto sedimentary deposits from the Eocene (Figure 1). The oldest formations found within the TMB are represented by the Huayacocotla and Cahuasas Formations, dating back to the Toarcian and Callovian ages, respectively (Figure 1). The Huayacocotla Formation, is mainly composed of quartz-rich conglomerates and sandstones, originated in a continental basin (Esquivel-Macías *et al.*, 2017). In contrast, the Cahuasas Formation is composed of conglomerates, sandstones, siltstones, and shales reflecting a fluvial and alluvial depositional environment (López-Infanzón, 1986). This continental phase ended-up with the deposition during the Middle Jurassic of, wackestone, anhydrite mudstone, and anhydrite, composing the Huehuetepec Formation (Nava-Pérez & Alegría-Luna, 2001). Subsequently, the Upper Jurassic units known as the Pimienta, Tamán, and Tepexic-Santiago formations show radical changes in composition with the presence of limestones, carbonaceous mudstones, and shales rich in organic matter. Concurrently, oolitic limestones, likely deposited at the basin margin, can be found in the San Andrés Formation (Todd, 1976). Predominant Sedimentary facies recorded during the Cretaceous are that of basin and oceanic shelf, with carbonate reefs developing on paleogeographic summits (López-Doncel, 2003; Rodríguez–Hernández, 2007). This entire period is characterized by gentle and prolonged subsidence. The lower part of the Tamaulipas Formation marks a transition phase during the Early Cretaceous, beginning with grainstones (oyster shape) and packstones interspersed with layers composed of bentonite and shale, and gradually transitioning to thicker limestone units upward (Hernández-Romano *et al.*, 1997). Maximum estimated subsidence depth occurred during the Albian-Cenomanian, with oceanic basin deposition facies. The upper part of the Tamaulipas Formation comprises limestones and shales of argillaceous and calcareous compositions, respectively. Early Cretaceous is represented by Santuario, Tamabra, El Abra, and Tamaulipas calcareous and carbonaceous formations. While the Santuario Formation mainly consists of limestones (dark-gray color), calcarenites, greywackes, and phyllitic shales (Segerstrom, 1962), the other formations are primarily composed of limestones. Notably, the Tamabra Formation includes interbedded calcareous breccia, the el Abra Formation features thick-bedded limestone, and the Tamaulipas Formation exhibits limestones with chert lenses and some evaporites at its bottom (Guaxcama Fm.). The Agua Nueva Formation (Early Turonian) is characterized by limestones enriched in clay and carbonates as well as calcareous shales. Formations known as San Felipe and Méndez are also very similar to Agua Nueva although they exhibit bentonite intercalations (Seibertz, 1986). During the Paleogene, the dominant sedimentary facies became siliciclastic, comprising a thick sequence of landslides, debris flows, and turbiditic flows that filled foreland basin of the Sierra Madre Oriental. These units are called Velasco, Chicontepec, and Guayabal formations (after Barker and Berggren, 1977). This period is also represented by the formation of the Bejuco-La Laja paleo-canyon and the Chicontepec paleo-channel (Santillán-Piña & Aguayo-Camargo, 2011). The upper portion of the overall detritic sequence, spanning from the Oligocene to the Recent, is composed of interbedded sandstones and shales, illustrated by Tantoyuca, Chapopote, Horcones, Palma Real, Mesón, and Tuxpan formations (Guzmán-Arellano, 2012).

The sedimentary column of the TMB also shows some magmatic intrusions of Middle Eocene to Quaternary ages associated with the Eastern Mexican Alkaline Province (EMAP). In the northern part of the TMB, as well as in Tamaulipas highs, these intrusions primarily consist in porphyritic and equigranular bodies, with minor hypabyssal igneous bodies, dating between approximately 44 and 20 million years ago (Hamblock, 2002; Pindell, 2009; Zhou -Décida *et al.*, 2009). Later (< 16 million years ago) prevalent lava flows and dikes have been reported within the basin (Ferrari *et al.*, 2005). East of the TMB lies the Aldama Volcanic Field, composed of alkali basalts and derived olivine trachytes from the Pliocene to the Pleistocene exhibiting geochemical signatures typical of intraplate magmatism (Camacho-Angulo, 1993; Aranda-Gómez *et al.*, 2005). Finally, the Llera de Canales Volcanic Field, located west of the Sierra de Tamaulipas and contemporaneous with the Aldama Volcanic Field, reports some basanitic lava flows, some alkaline basalts, and sodic trachybasalts (*i.e.* hawaiites) lava flows (Aranda-Gómez *et al.*, 2005 and references therein). Viera-Décida *et al.* (2009) also suggested that the igneous rocks from Palma Sola and from Los Tuxtlas that have been emplaced during the Late Upper Oligocene to Miocene, at the southern border of the TMB, may represent the southernmost extent of the EMAP.

RESERVOIR CHARACTERIZATION

Comisión Nacional de Hidrocarburos (CNH, 2018) data from oil wells penetrating the Jurassic column were used to characterize the petrophysical properties of the target saline aquifers. Regional 3D seismic reflection surveys are combined with detailed well-log analyses from Pemex-PEP exploration wells. Lithology mudlogs, which describe the main rock types within specific depth intervals, are constructed using core descriptions. These descriptions encompass key features such as grain size, mineralogy, grain distribution, matrix composition, density, and fluid content.

Wells selection

Five wells—Planos-1, Palmar-1, Tablon-1, Defense-1, and Tecomate-1—met the primary selection criteria: availability of geological and petrophysical data, and penetration into the Jurassic sedimentary sequence within the seismic survey area (Figures 2 and 3). These wells encountered the reservoir Jurassic formations at depths ranging from 3200 to 4900 meters below the surface. Penetration depth into the Jurassic formations varied among the wells. All five wells intersected the uppermost 500 to 600 meters of the Jurassic column. The Cahuasas Formation, characterized by sandstone lithology, constitutes the top of the Jurassic sequence. This formation maintains a relatively consistent thickness of approximately 400 meters across the Coyula 3D seismic block. Overlying the Cahuasas sandstone is the Huehuetepec Formation, composed of Upper Jurassic shale. Notably, the base of the Huehuetepec Formation contains discontinuous evaporite layers. These evaporite layers serve as both a reliable marker horizon for stratigraphic and petrophysical correlation and an effective caprock due to their distinct geological and petrophysical properties.

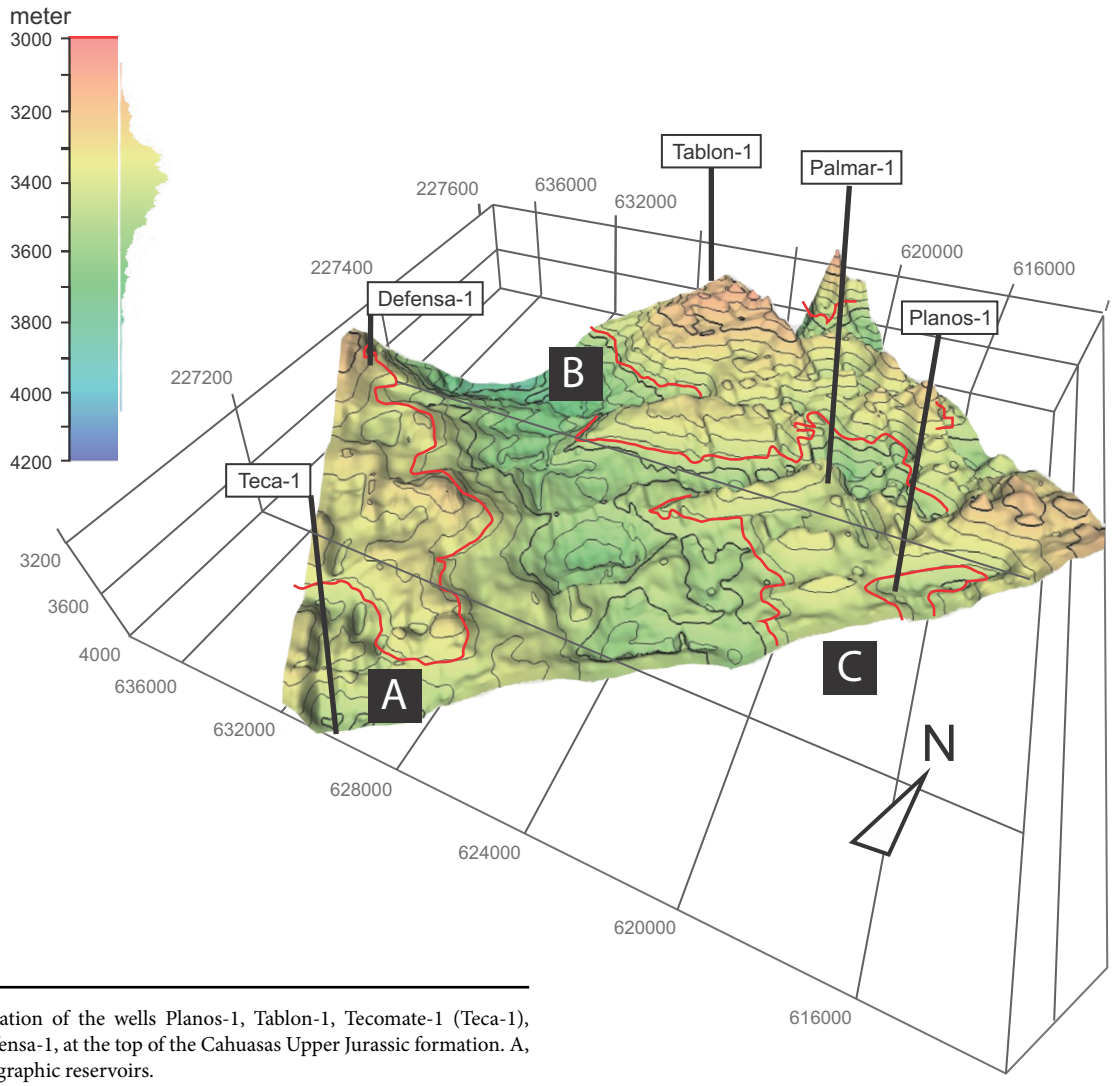


Figure 2. Location of the wells Planos-1, Tablon-1, Tecomate-1 (Teca-1), Palmar-1, Defensa-1, at the top of the Cahuasas Upper Jurassic formation. A, B and C stratigraphic reservoirs.

The seismic model and reservoir volume estimation

A lithostratigraphic-structural model of the study area was constructed using Petrel® software (version 2013). The 3D seismic reflection cube was calibrated using data from the five positioned well logs. Regional interpretation of the seismic data, with a 25-meter profile spacing, made it possible to identified key stratigraphic horizons and faults. Following digitization and interpretation (2D), the faults and stratigraphic tops were converted into surfaces, forming the basis of the 3D stratigraphic-structural model. Linear interpolation was employed for this conversion. To estimate reservoir volume, a 3D geocellular model was built using the interpreted structural and stratigraphic data from the depth-converted 3D seismic cube. Geological contacts defined using well log data, lithological descriptions, and paleontological reports, guided the interpretation of surfaces and faults. This interpretation informed the creation of a structural model with sub-horizons and faults, which was then used to generate a 3D orthogonal cell grid comprising 225600 cells and 237456 nodes. Petrophysical properties, including porosity and permeability, were extrapolated through the 3D cell grid using geostatistical methods constrained by interval velocity and validated with core measurements. Finally, a geometric volume was calculated for each cell, and an index filter was applied to delineate the prospective reservoirs

Petrophysical properties

Porosity and permeability

Porosity and permeability were initially determined from well-log measurements and then validated against core sample analyses from Tecomate-1 well to ensure accurate representation of these well-log reservoir properties (Figure 4). Two methods, Wyllie Time Average (sonic porosity) and Neutron porosity, were employed to estimate porosity. Permeability was determined using the Wyllie-Rose method for sands and the Coates and Dumanoir method for fine-grained facies (Wyllie and Rose, 1950; Coates and Dumanoir, 1974). Notably, the sonic porosity and Wyllie-Rose permeability estimations demonstrated good agreement with helium porosity and steady-state permeability measurements conducted on core samples from the Tecomate-1 well. These core samples, extracted from calcareous sandstone facies at the top of the Cahuasas Formation, provided valuable ground truth data. Furthermore, a lithological index, integrating porosity and permeability information, was interpreted to classify the predominant facies within the Tamán, Tepexic, Santiago, and Cahuasas formations, enhancing the understanding of reservoir heterogeneity (Figure 5).

Vertical stress and pore pressure profiles

The vertical stress profile was determined using a combination

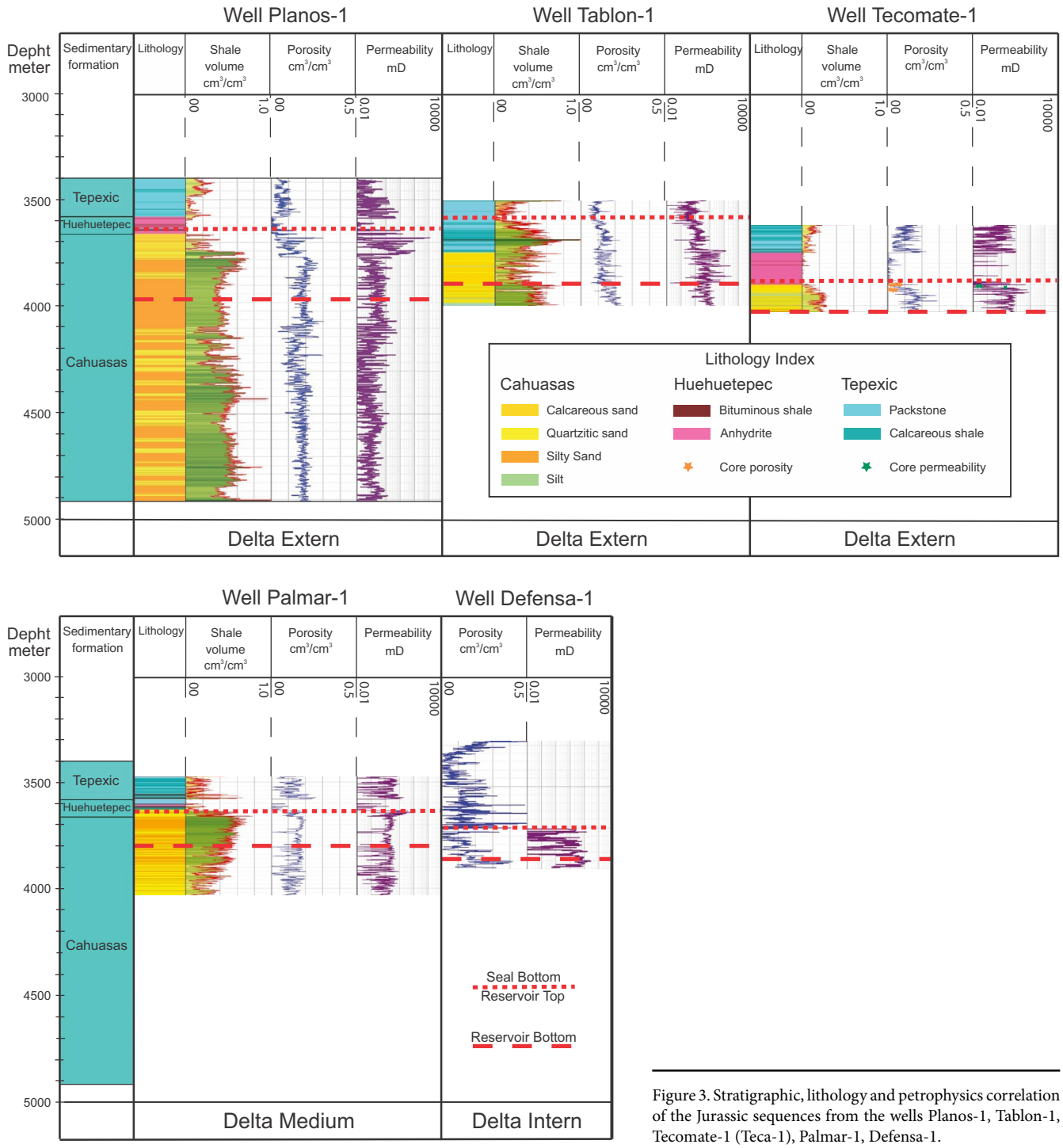


Figure 3. Stratigraphic, lithology and petrophysics correlation of the Jurassic sequences from the wells Planos-1, Tablon-1, Tecomate-1 (Teca-1), Palmar-1, Defensa-1.

of bulk density logs and extrapolated density estimations for shallow intervals where log data might be limited. Vertical pore pressure profiles were estimated using the Eaton method, which utilizes compressional slowness logs (Eaton, 1972). These estimations were then validated against mud density profiles and gas reports for accuracy. Mud-loss pressure profiles were estimated using the Matthews and Kelly (1967) method, assuming a ratio of 0.75 between the vertical stress and the minor horizontal stress. This assumption is often used in regions with limited stress data. These estimations were further validated against mud-loss and ballooning events documented in drilling reports from five offset wells, providing valuable insights into actual wellbore conditions. The use of offset well data enhances the reliability of the mud-loss pressure profile.

Dynamic elastic modulus

The dynamic elastic modulus was determined using density and sonic log data (compressional and shear). Where density log data were unavailable, a correlation between compressional sonic and density logs, tailored to the specific lithological facies, was employed. The shear sonic log, a key component in calculating the

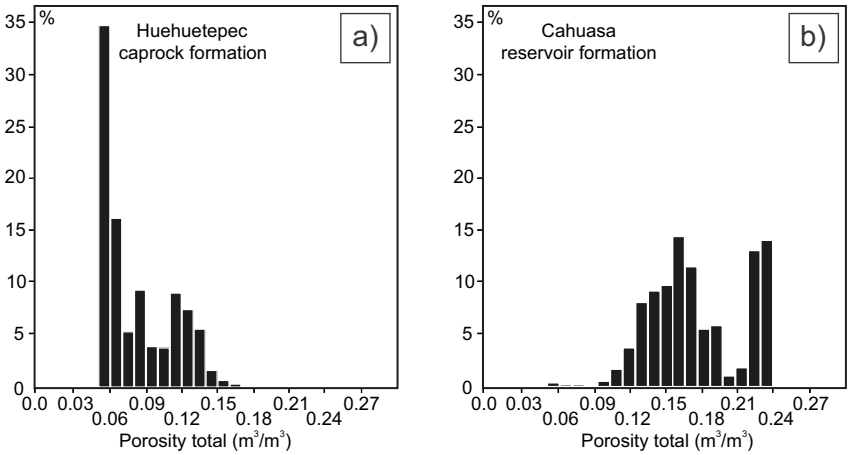


Figure 4. Porosity values distribution of the upper part of a) the Huehuetepec caprock formations and b) the Cahuasas reservoir section from the Tecomate-1 well.

dynamic elastic modulus, was estimated using Castagna *et al.* (1985) relations for saturated sandstones and shales. This approach leverages the relationship between compressional and shear wave velocities in different lithologies. It is important to note that the dynamic elastic modulus, estimated from acoustic wave propagation in an isotropic elastic medium, is typically higher than the static elastic modulus. This difference arises because dynamic measurements, acquired under dynamic conditions, involve smaller deformation amplitudes compared to static measurements.

Effective storage capacity estimation

Structural highs, representing structural traps, were identified as potential CO_2 storage sites. This selection was based on the positive buoyancy of CO_2, which tends to migrate upwards, and the presence of coarse-grained alluvial fan deposits (sandstones) within these structures, providing suitable reservoir characteristics. However, due to limited data on the hydraulic properties (specifically, transmissivity) of the faults bounding these potential reservoirs, two boundary condition scenarios were considered, open and closed systems. A closed system assumes that faults behave as sealing boundaries, effectively compartmentalizing the reservoir and restricting fluid flow to the defined structural closure. In contrast, an open system allows for hydraulic connectivity with adjacent stratigraphic or structural units, enabling pressure dissipation and fluid exchange across boundaries. Evaluation of these end-member scenarios constrains the envelope of possible system behaviors and supports a more rigorous quantification of volumetric capacity and dynamic uncertainty. The closed system represents the most conservative, capacity-limited scenario.

Open system

To estimate the effective storage capacity of the identified geological structures as open systems, we employed the DOE methodology with a probabilistic approach. This approach utilizes effectiveness coefficients representing the P10, P50, and P90 percentiles for parameters influencing storage capacity (U.S. DOE, 2007). The total CO_2 storage capacity ($G_{CO2}T$) is calculated using the following equation:

$$G_{CO2}T = A \text{ x } h \text{ x } \Phi \text{ x } \rho CO_2 \text{ x } E_E \quad (1)$$

where:

A: reservoir area (given in m², obtained from seismic and petrophysical data (Figures 5 and 6)).

h: reservoir thickness (given in m, obtained from seismic and petrophysical data (Figures 5 and 6)).

Φ: porosity (given in m^3/m^3, calculated from well logs and laboratory analyses (Figure 6)).

ρCO_2: CO_2 density (given in kg/m^3, estimated based on reservoir depth and temperature).

E_E: efficiency coefficient (calculated using Equation 2).

To estimate realistic values for the storage capacity of the specific reservoirs (A, B, C, Figure 5), we decide to use the most conservative characteristic values for the different horizon in the considered properties.

The efficiency coefficient (E_E) represents the combined effect of geological, volumetric, and microscopic displacement efficiencies (IEA-GHG, 2009):

$$E_E = E_{Geol} \text{ x } E_V \text{ x } E_d \quad (2)$$

E_{Geol} is the geological efficiency (dimensionless). This factor accounts for the portion of the geological unit suitable for CO_2 storage, considering net area, net thickness, and effective porosity:

$$E_{Geol} = (A_n/A_t) \text{ x } (h_n/h_g) * (\Phi_{ef}/\Phi T) \quad (3)$$

where:

A_n (Net area): expressed in square meters (m²).

A_t (Total area): expressed in square meters (m²).

A_n/A_t : net-to-gross area ratio (dimensionless), determined from petrophysical models using a minimum total porosity cut-off of $\Phi T = 0.10$; (Hatzignatiou *et al.*, 2011).

h_n/h_g: net-to-gross thickness ratio (dimensionless), derived from well logs using a clay volume cut-off of 0.20; thickness values are expressed in meters (m; Figures 5 and 6).

Φ_{ef} (Effective porosity)**:** expressed as a fraction or percentage (v/v). It represents the interconnected pore space available for fluid flow and storage (dimensionless).

ΦT (Total porosity)**:** expressed as a fraction or percentage (v/v). It includes both connected and isolated pores, as well as bound water associated with clays (dimensionless).

$\Phi_{ef}/\Phi T$: effective porosity fraction (calculated from petrophysical logs, (Figure 3)), dimensionless (fraction), indicating the proportion of the total pore space that effectively contributes to fluid flow or storage.

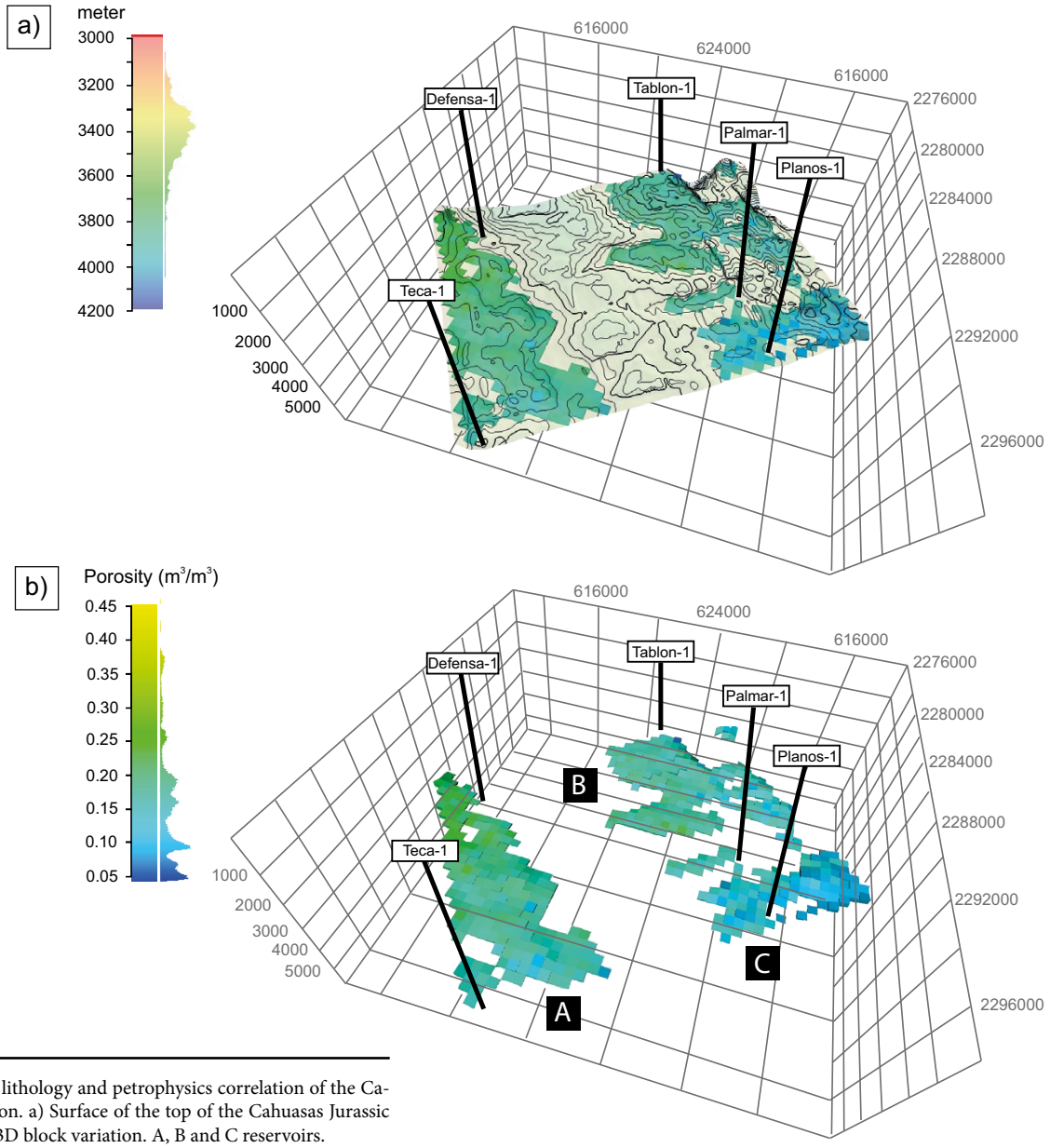


Figure 5. Stratigraphic, lithology and petrophysics correlation of the Cahuasas Jurassic formation. a) Surface of the top of the Cahuasas Jurassic formation. b) Porosity 3D block variation. A, B and C reservoirs.

E_v (volumetric displacement efficiency) represents the fraction of pore space accessible to CO_2 injection. Due to limited data on reservoir heterogeneity, E_v values were derived from the IEA-GHG (2009) report (Appendix E corresponding to sandstones of an alluvial fan depositional environment).

E_d (efficiency of microscopic displacement) represents the fraction of pore space where CO_2 can effectively displace the existing fluids (*e.g.*, water). It is calculated using the following equation (Bassiouni, 1994):

$$E_d = 1\text{-}S_{wirr}$$

and:

$$S_{wirr} = \sqrt[n]{\frac{aRw}{\Phi T^{m} Rt}}, \quad (4)$$

where:

S_{wirr}: irreducible water saturation (the fraction of pore space occupied by immobile water, dimensionless).

Rw: water resistivity (given in Ohmmeter, obtained from well logs).

ΦT: total porosity (obtained from well logs, dimensionless).

Rt: deep penetration resistivity (given in Ohmmeter, obtained from well logs).

a, *m*, *n*: Empirical constants (dimensionless).

For this study, the following values were used based on the lithology (carbonate rocks: a = 1, m = 2, n = 2; silicoclastic rocks: a = 0.62, m = 2.15, n=2 (Table 1; Archie, 1942).

These parameters, along with the well log data, allow for the calculation of E_d, which contributes to the overall efficiency coefficient for estimating CO_2 storage capacity (Table 2).

Close systems

For closed systems, where CO_2 migration is restricted, the storage capacity calculation considers the compressibility of the rock and fluids. The equation for total CO_2 storage capacity in a closed system is:

$$G_{CO2}T = A \text{ x } h \text{ x } \Phi \text{ x } \rho CO_2 \text{ x } E_{comp} \quad (5)$$

where:

Φ: porosity (given in m^3/m^3, calculated from well logs and laboratory analyses, Figure 6).

ρCO_2: CO_2 density (given in kg/m^3, estimated based on reservoir depth and temperature).

E_{comp}: compressibility effectiveness coefficient (given in MPa, calculated using Equation 6).

This coefficient accounts for the volumetric changes due to the compressibility of rock and water under increased pressure from CO_2 injection. It is calculated as follows (Zhou *et al.*, 2008; U.S. DOE, 2007):

$$E_{comp} = (\beta r + \beta a)\Delta p \quad (6)$$

where:

βr: rock compressibility (calculated as $1/K$, where K is the compressibility modulus obtained from the petrophysical model).

βa: water compressibility (assumed constant at 4.6e-10 Pa^{-1}).

Δp: $(P_p - P_f)$ pressure increase, where P_p is pore pressure, P_f is the pressure of fracturation (using the synthetic curves of effective porosity and DTCO measurements for each horizon of interest in the reservoirs (Eaton, 1975; Bowers 1995)).

The rock compressibility is determined by the relationship βr $1/K$. The compressibility modulus K was obtained in each of the horizons of interest from the petrophysics model (Zimmerman, 1991; Ahmed, 2006; Table 1). The water compressibility (βa) is considered a constant (4.6 e^{-10} Pa^{-1}; EIA-GHG, 2009).

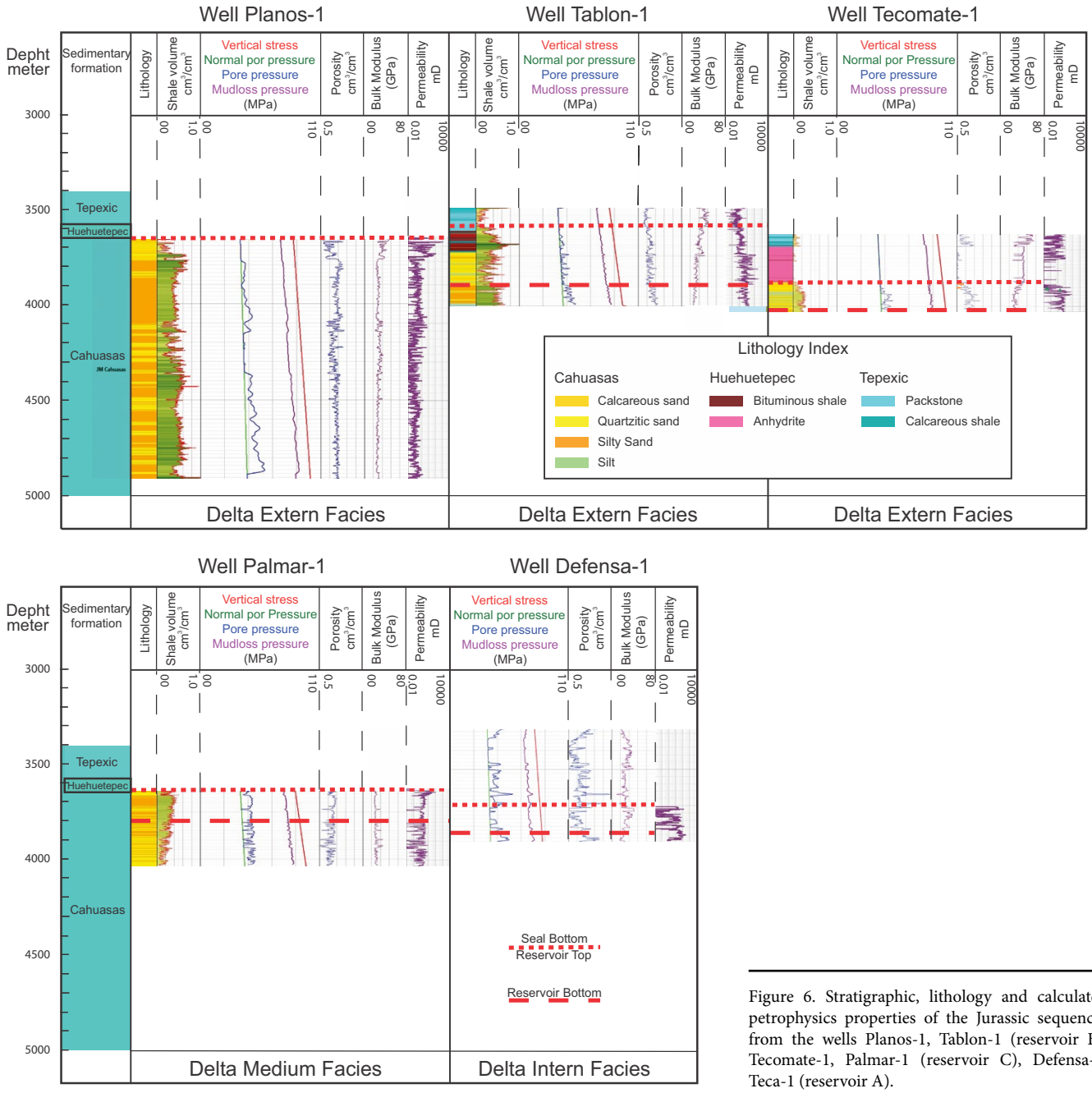


Figure 6. Stratigraphic, lithology and calculated petrophysics properties of the Jurassic sequences from the wells Planos-1, Tablon-1 (reservoir B), Tecomate-1, Palmar-1 (reservoir C), Defensa-1, Teca-1 (reservoir A).

Table 1. Synthesis of petrophysics characteristics determined for each stratigraphy level for the different reservoirs (A, B, C).

	Well	Depht (m)	Overpressure (MPa)	Pore pressure (MPa)	Fracture pressure (MPa)	Compressibility mode (K)	Porosity (m^3/m^3)	Permeability (mD)
Reservoir - A	Tecoman-101	3900–3940	92.6	39.9	87.6	26.6	0.08	0.26
	Tecoman-101	3950–4025	94.5	40.7	90.8	26.2	0.16	2.4
	Defensa-101	3600–3650	84.1	36.9	72.8	24.2	0.07	0.52
	Defensa-101	3665–3690	85.4	47.2	76.4	22.4	0.2	2.5
Reservoir - B	Planos-1	3580–3620	86.2	36.9	75.8	36.3	0.08	0.6
	Planos-1	3800–3900	91.9	42.1	80.9	27.9	0.14	0.02
	Planos-1	4000–4050	96.1	49.0	85.1	22.6	0.17	0.13
Reservoir - C	Tablón-1	3730–3760	89.2	41.7	77.7	26.9	0.13	6.05
	Tablón-1	3790–3890	91.2	39.1	76.7	27.4	0.12	5.99
	Tablón-1	3930–3990	94.8	47.1	83.4	23.6	0.18	5.47
	Palmar-1	3630–3660	88.1	40.8	76.8	23.9	0.11	5.82
	Palmar-1	3800–3850	92.3	49.5	82.3	21.1	0.13	0.82
	Palmar-1	3950–4000	95.8	48.0	84.7	23.2	0.14	1.05
	***K* (*Pa*)**	***βr* (*1/K*)(*Pa*$^{-1}$)**	***βa* (*Pa*$^{-1}$)**	***Pf* (*Pa*)**	***Pp* (*Pa*)**	***ΔP* (*Pa*)**	***βa*+*βr* (*Pa*$^{-1}$)**	E_{comp}
Reservoir - A	26593000000	3.76039E-11	4.6E-10	87563000	39918000	47645000	4.97604E-10	0.024
	26163000000	3.82219E-11	4.6E-10	90785000	40726000	50059000	4.98222E-10	0.025
	24213000000	4.13001E-11	4.6E-10	72839000	36851000	35988000	5.013E-10	0.018
	22420000000	4.4603E-11	4.6E-10	76370000	47169000	29201000	5.04603E-10	0.015
Reservoir - B	36254600000	2.75827E-11	4.6E-10	75759000	36895300	38863700	4.87583E-10	0.019
	27948000000	3.57807E-11	4.6E-10	80949000	42114000	38835000	4.95781E-10	0.019
	22571000000	4.43046E-11	4.6E-10	85092000	48973000	36119000	5.04305E-10	0.018
Reservoir - C	26872000000	3.72135E-11	4.6E-10	77651000	41659000	35992000	4.97213E-10	0.018
	27430000000	3.64564E-11	4.6E-10	76682000	39076000	37606000	4.96456E-10	0.019
	23613000000	4.23496E-11	4.6E-10	83396000	47136000	36260000	5.0235E-10	0.018
	23930100000	4.17884E-11	4.6E-10	76846000	40843200	36002800	5.01788E-10	0.018
	21085000000	4.74271E-11	4.6E-10	82262000	49463000	32799000	5.07427E-10	0.017
	23186000000	4.31295E-11	4.6E-10	84736000	48046000	36690000	5.03129E-10	0.018

DETERMINATION OF EFFECTIVE STORAGE CAPACITY IN SELECTED AREA

The CO_2 storage capacity for the Cahuasas Upper Jurassic formation within the Coyula seismic block was calculated based on the lithology and the petrophysical properties of the five exploratory oil wells crossing the seismic block. Three main reservoirs were identified (A, B, C in Figure 5). All the reservoirs are sealed by a thick efficient caprock composed of shale and evaporite characterized for their very low permeability (Figure 4). The trapping mechanism involves stratigraphic trapping through lateral delta and alluvial fan facies variations. Figures 5 shows the reservoirs A, B, C depth range from 3600 to 3900 m. The three reservoirs present the same lithology made off sandstone with shaly layers intercalation. For accuracy, the CO_2 density is estimated as a density range, following the reservoir depth and thickness and reservoir temperature variation (Medina *et al.*, 2023). The full data set use to develop the Equation 1 for open system and Equation 5 for close system are summarized in Table 1. We estimated the CO_2 potential storage resources for each Cahuasas stratigraphic layers of the three reservoirs (A, B, C). The range of the petrophysics characteristics are comparable in all reservoirs. The pore and fracture pressures vary from 36.9 to 46.5 MPa and from 72.8 to 90.8 MPa respectively. The reservoir A shows wider porosity and relative homogeneous permeability varying from 0.07 to 0.2 % and 0.26 to 2.5 mD, compared to B and C reservoirs, ranging from 0.12 to 0.18 % and from 0.2 to 6.5 mD. Irreducible water values varied between 47 to 60 %. The density of CO_2 is estimated as a min and max range from 417 to 663 kg/m^3, considering the reservoir temperature and lithologic pressure. The reservoir volumes are underestimated and still comparable (Table 2). The volumes of reservoirs A and B are constrained by the lateral extent of the seismic blocks rather than by stratigraphic closure (Figure 5).

For the determination of the effective storage coefficients in a closed system hypothesis, the porosity is presented as a weighted mean by reservoirs. The efficiency coefficient (E_E) estimate for each reservoir is comparable ranging from 1.79 (reservoir C) to 2.03 (reservoir A). The effective storage capacities of CO_2 are estimated as a minimum and maximum range. The results are presented in volumetric and mass effective storage capacity (Table 3). The ranges vary from 3.83 to 6.09 Mton for reservoir A, from 4.93 to 7.83 Mton for reservoir B, and from 7. 63 to 11.70 Mton for reservoir C, for a total at the Coyula seismic block ranging from 16.11 to 25.62 Mton CO_2. The most impacting data in the final CO_2 mass estimation is the reservoir volume.

For the open system hypothesis, we used the same petrophysical data than previously. We estimate efficient coefficients for open system for a sedimentary environment of sandstone deposited in an alluvial fan with a monoclinal structure, shown in the Table 4 for the 10, 50, and 90 percentiles (P; Tables 1 and 4).

The results are presented in volumetric and mass effective storage capacity. Geological and petrophysical data vary in comparable way in the three reservoirs. Reservoir volume and the associated percentiles represent the key parameters that exert the greatest influence on

Table 2. CO_2 storage potential for the Coyula Block, for a close system hypothesis. Results are presented by reservoirs (A, B, C).

Close system	***Volume* (*V*)** (m^3)	**ϕ** (average)	**Density (ρ) CO_2** (g/cm^3)		**E_{comp}**	**Effective storage capacity Volume** (m^3) **($V\phi^* E_{comp}$) average**	**Effective storage capacity Mass Mton ($V\phi^* E_{comp}{}^* \rho$)**	
			Min.	Max.	Average	Effective storage capacity. Volume m^3 ($V\phi^* E$)	Min.	Max.
Reservoir - A	3549127186	12.75	417	663	2.03	9186028.439	3.83	6.09
Reservoir - B	4832742533	13			1.88	11811222.75	4.93	7.83
Reservoir - C	7300852499	13.50			1.79	17642510.06	7.36	11.70
Total							**16.11**	**25.62**

the final storage potential estimation (Table 4). The maximum and minimum effective storage capacity obtained for the reservoirs in the Coyula block range from 11.21 to 17.28 Mton (P10) to 27.32 to 43.44 Mton (P90) for reservoir A, from 3.8 to 6.16 Mton (P10) to 9.69 to 15.41 Mton (P90) for reservoir B, and from 10.56 to 16.79 Mton (P10) to 38.35 to 60.97 Mton (P90) for reservoir C, for a total estimation at Coyula block of 25.65 to 40.78 Mton (P10) to 75.36 to 119.82 Mton (P90). We consider these values a conservative estimate for the potential of the Cahuasas sandstone.

When compared with capacity estimates from some of the most extensively studied CO_2 storage projects worldwide—such as Quest and Weyburn in Canada, Cranfield in the USA, Sleipner in Norway, and Gorgon and Otway in Australia—the results obtained in this study appear both consistent and promising. These reference sites span a range of geological contexts, including deep saline aquifers (*e.g.*, Sleipner, Quest, Gorgon, Otway) and depleted or producing hydrocarbon reservoirs (*e.g.*, Weyburn, Cranfield), providing a robust benchmark for comparison.

In terms of storage capacity, these projects typically range from several tens to hundreds of millions of tonnes of CO_2. For instance, Sleipner has been injecting approximately 1 million tonnes of CO_2 per year since 1996 into a saline aquifer (Furre *et al.*, 2017), while Gorgon represents one of the largest projects globally, with planned storage on the order of hundreds of millions of tonnes (Weijmars, 2024). Similarly, Quest has stored several million tonnes of CO_2 in a deep saline formation, and Weyburn and Cranfield demonstrate significant storage potential in carbonate and sandstone reservoirs associated with hydrocarbon systems (White, 2011). These sites are characterized by well-constrained structural or stratigraphic traps, adequate reservoir quality (porosity and permeability), and effective sealing formations.

Within this global context, the capacities estimated in the present study fall within a comparable order of magnitude, considering the scale of evaluation and available data. The geological setting, involving sedimentary formations with suitable petrophysical properties and structural configurations, further supports the relevance of the comparison. Although uncertainties remain—particularly related to data density and model resolution—the results suggest that the studied reservoirs share key characteristics with established storage sites.

MODEL UNCERTAINIES

Effective capacity is typically estimated using probabilistic volumetric approaches that incorporate storage efficiency coefficients derived from numerical simulations and calibrated with petrophysical data. Such methods allow the integration of geological variability and uncertainty, providing a range of possible storage values rather than a single deterministic estimate. Effective capacity thus represents a more realistic and operationally relevant assessment of storage potential and serves as an intermediate metric between theoretical and practical capacities, particularly useful for site screening and early-stage evaluations (CSLF, 2007; U.S. DOE, 2007; Bachu, 2003; IEA-GHG, 2009).

A major challenge in estimating effective capacity lies in the quantification of uncertainties, especially those related to seismic interpretation and interpolation of reservoir properties. Seismic data define reservoir geometry and structure but are affected by resolution limits, velocity model uncertainties, and interpretation subjectivity. These uncertainties propagate into key volumetric parameters such as thickness and reservoir extent and are further amplified during time-to-depth conversion in heterogeneous formations. Similarly, the interpolation of petrophysical properties between wells introduces additional uncertainty. Given these cumulative uncertainties, deterministic values can be misleading. A probabilistic framework is therefore essential, where uncertainty is propagated through volumetric calculations to generate distributions of storage capacity. The use of statistical percentiles (P10, P50, P90) allows the definition of reliable ranges, with P50 representing the most likely value and P10–P90 bounding optimistic and conservative scenarios. Expressing

Table 3. Petrophysical estimation for the Coyula Block, for an open system hypothesis. Results are presented by reservoirs (A, B, C).

Close system	***Volume* (*V*)** (m^3)	**ϕ** (average)	**Density (ρ) CO_2** (g/cm^3)		**E_{comp}**	**Effective storage capacity. Volume** (m^3) **($V\phi^* E_{comp}$) average**	**Effective storage capacity Mass Mton ($V\phi^* E_{comp}{}^* \rho$)**	
			Min.	Max.	Average	Effective storage capacity. Volume m^3 ($V\phi^* E_{comp}$)	Min.	Max.
Reservoir - A	3549127186	12.75	417	663	2.03	9186028.439	3.83	6.09
Reservoir - B	4832742533	13			1.88	11811222.75	4.93	7.83
Reservoir - C	7300852499	13.50			1.79	17642510.06	7.36	11.70
Total							**16.11**	**25.62**

Table 4. CO_2 storage potential for the Coyula Block, for an open system hypothesis. Results are presented by reservoirs (A, B, C).

ID	*Volume* (*V*) (m^3)	ϕ	Density (ρ) CO_2 (g/cm^3)		E_E (%)			Effective storage capacity Volume m^3 ($V\phi^*E_E$)			Effective storage capacity Mass Mton ($V\phi^*E_E{}^*\rho$)					
			Min.	Max.	P10	P50	P90	Min.	50	Max.	Min.		50		Max.	
											417	663	417	663	417	663
Reservoir - A	3549127186	12.75	417	663	5.94	9.4	14.48	26879314.7	42536289.32	65523986.11	11.21	17.82	17.74	28.20	27.32	43.44
Reservoir - B	4832742533	13			1.48	2.04	3.7	9298196.63	12816433.2	23245491.58	3.88	6.16	5.34	8.50	9.69	15.41
Reservoir - C	7300852499	13.5			2.57	3.71	9.33	25330307.7	36566319.74	91957887.65	10.56	16.79	15.25	24.24	38.35	60.97
Total											**25.65**	**40.78**	**38.33**	**60.94**	**75.36**	**119.82**

storage capacity as percentile ranges provides a robust and transparent basis for risk-informed decision-making, particularly in early-stage assessments where data limitations are significant.

SUMMARY AND CONCLUSION

The Cahuasas Upper Jurassic formation in the Coyula seismic block shows promising characteristics for CO_2 storage, including permeable strata sealed by impermeable layers at depths suitable for injection (3500 – 4000 m). Identified saline aquifers exhibit high permeability (0.2 – 6.05 mD for sandstone and clay intercalations) and porosity ranging from 0.07 % to 0.2 %, making them suitable for CO_2 storage. These layers are suitable reservoir rocks qualified for permanent CO_2 storage. The CO_2 storage potential in the Cahuasas formation at the Coyula block was calculated based on the rock compositions and petrophysical properties from exploratory oil wells. Three stratigraphic reservoirs, called A, B and C were identified sealed by Huehuetepec shale formation. The prospective storage resources of the three reservoirs were calculated locally, integrating seismic profiles and wells data considering the open and close systems hypothesis. In this case the close system will be the most conservative results (16.11 to 25.62 Mton CO_2) as a first site evaluation. This study suggests that the CO_2 storage capacity ranges approximately for open system from 25.65 to 40.78 Mton (lower range), and 75.36 to 119.82 Mton (maximum conditions). Summing the three Cahuasas formation reservoirs, the geological storage efficiencies range from 0.08 % to 4.3 %. The results obtain from the close system hypothesis are comparable to the lower characteristic ranges (P10) of the open system. The Cahuasas formation within the Coyula block, representing less than 10 % of the Tampico Misantla basin, demonstrates significant CO_2 storage potential, exceeding the estimated annual CO_2 emissions from the basin's oil industry (approximately 4 Mton; Medina *et al.*, 2023).

The uncertainty associated with subsurface data gaps was incorporated into the storage resource evaluation due to the legacy of seismic data and the relatively limited well data available over the study area. As well, the upper Jurassic reservoirs show evidence of alluvial fan geometry and natural permeability heterogeneity and/or reactivation structures (Figure 1, Aguayo-Camargo *et al.*, 2018). Jurassic faults and lateral permeability variation are potentially boundaries defining a "semi-closed system" from which the lateral displacement of brine during CO_2 injection might be prevented and contained, avoiding a pressure buildup in the reservoir (*e.g.*, Zhou *et al.*, 2008).

Overall, the comparison with reference sites indicates that the storage potential identified is credible and sufficiently robust to justify advancing to the next stage of detailed evaluation. This should include refined geological and dynamic modeling, improved constraint of petrophysical parameters, and a more comprehensive uncertainty assessment, in order to better define injectivity, containment, and long-term storage performance.

Acknowledgments. This research is part of the first author's PhD project in the framework of the Universidad Nacional Autónoma de México (UNAM) Postgraduate Program. The research was funded by SENER-CONACYT grant CB-263486 to G. Levresse. We are grateful to the Comision Nacional de Hidrocarburos, and the Secretaria de Energia for the technical support and data access through the ARES-NVR-MX-16-4Y8 agreement.

Author contributions. Erik Medina: Methodology, investigation, data processing, analysis and interpretation, writing, Gilles Levresse: Methodology, investigation, data processing, analysis and interpretation, writing,, Cesar A. Cortes-Prado: data processing, analysis and interpretation, review, Mariano Cerca: Methodology, formal analysis, review, Jaime Carrera-Hernandez: Review and investigation, Berengere Mougel: Review and investigation. All authors discussed the results and contributed to the writing of the manuscript.

Data availability statement. The authors declare that the data supporting the findings of this study are available upon request from GL. The data are not publicly available due to confidential agreement with CNH.

Declaration of competing interest. The authors declare that they have no known competing financial interests or personal relationships that could have appeared to influence the work reported in this paper.

Funding: CONACYT grant CB-263486.

REFERENCES

Aguayo-Camargo, J. E., Noé Santillán-Piña, N., & Arellano-Gil, J. (2018). Prograding low-density turbidite systems and oil traps at the Lower Paleogene Chicontepec Foreland Basin, East-Central Mexico. *Ingeniería, investigación y tecnología*, *XIX*(4), e035.

Ahmed, A. J. (2006). Compressibility of porous rocks: Part II. New relationships. Petroleum Engineering Department. *Acta Geophysica, 54*(4), 399–412. https://doi.org/10.2478/s11600-006-0029-4

Al-Khoury, R., & Bundschuh, J. (2014). *Computational Models for CO_2 Geo-sequestration and Compressed Air Energy Storage*. Taylor & Francis.

Aranda-Gómez, J. J., Housh, T. B., Luhr, J. F., Henry, C. D., Becker, T., & Chávez-Cabello, G. (2005). Reactivation of the San Marcos fault during mid- to late Tertiary extension, Chihuahua, México. In J.A. Nourse, T.H., Anderson, J.W., McKee, M.B., Steiner, (eds.), The Mojave-Sonora megashear hypothesis: Development, assessment, and alternatives: *Geological Society of America, Special Paper, 393*, 509–522. https://doi.org/10.1130/0-8137-2393-0.509

Archie, G. E. (1942). The Electrical Resistivity Log as an Aid in Determining Some Reservoir Characteristics. *Transactions of the AIME*, 146, 54–62.

Bachu, S. (2003). Screening and ranking of sedimentary basins for

sequestration of CO_2 in geological media in response to climate change. *Environmental Geology*, *44*, 277–289.

Barker, R. R. W., & Berggren,W. A. (1977). Paleocene ánd Early Eocene of the Rio Grande and Tampico Embayments: iferal biostratigraphy and paleoecology. *Marine cropaleontoiogy*, 2, 67–103.

Bassiouni, Z. (1994). Theory, Measurement and Interpretation of Well Logs Tulsa, Oklahoma, USA. *SPE Textbook Series 4*.

Bowers, G. L. (1995). Pore pressure estimation from velocity data: accounting for overpressure mechanisms besides under compaction. *SPE Drilling & Completion*, *10*, 89–95. doi: https://doi.org/10.2118/27488-PA

Camacho-Angulo, F. (1993). *Compilación geológica de la vertiente del Golfo de México: Veracruz, Ver*. Comisión Federal de Electricidad, Subdirección Técnica, Gerencia de Estudios de Ingeniería Civil, Subgerencia de Estudios Geológicos, Departamento de Geología, Zona Golfo, 169 pp.

Carrillo-Bravo, J. (1971). La Plataforma de Valles San Luis Potosí. *Boletín de la Asociación Mexicana de Geólogos Petroleros*, *23*, 102 pp.

Castagna, J., Batzle, M. L., & Eastwood, R. L. (1985). Reklationship between compressional and shear-wave velocities in classic silicate rocks. *Geophysics*, *50*, 571–581. DOI: 10.1190/1.1441933

Coates, G. R., & Dumanoir, J. L. (1974). A new approach to improved log derived permeability. *SPWLA Fourteenth annual logging symposium*, 1–28.

Coombs, H., Kerr, A., Pindell, J., Buchs, D., Weber, B., & Solari, L. (2020). Petrogenesis of the crystalline basement along the western Gulf of Mexico: Post-collisional magmatism during the formation of Pangea. In U. C. Martens, R. S. Molina Garza (Eds.), Southern and Central Mexico: Basement Framework, Tectonic Evolution, and Provenance of Mesozoic–Cenozoic Basins. *GSA Special Papers*, *546*, 29–52. https://doi.org/10.1130/2020.2546(02)

Comisión Nacional de Hidrocarburos (CNH; 2018). *Atlas geológico cuenca tampico-misantla. Versión 3*. Centro Nacional de Información de Hidrocarburos. https://hidrocarburos.gob.mx/media/3091/atlas_geologico_cuenca_tampico-misantla_v3.pdf

CSLF (2007). Estimation of CO_2 Storage Capacity in Geological Media. *Carbon Sequestration Leadership Forum, 43*.

Eaton, B. (1972). The Effect of Overburden Stress on Geopressure Prediction from Well Logs. *Journal of Petroleumt Technology*, *24*(8), 929–934. SPE-3719-PA. http://dx.doi.org/10.2118/3719-PA

Eaton, B. A. (1975). The Equation for Geopressure Prediction from Well Logs. Fall Meeting of the Society of Petroleum Engineers. *SPE 5544*, october, 1975. https://doi.org/10.2118/5544-MS

Eguiluz de Antuñano, S. (2011). Sinopsis geológica de la Cuenca de Burgos, noreste de México: producción y recursos petroleros. *Boletín de la Sociedad Geológica Mexicana*, *63*, 323–332.

Esquivel-Macías, C., León-Olvera, R. G., & Flores Castro K. (2017). Paleoenvironment and biostratigraphy of the Upper Sinemurian (Lower Jurassic) of the Huayacocotla Formation in East-Central Mexico. *Boletín de la Sociedad Geológica Mexicana*, *69*(3), 739–770. http://dx.doi.org/10.18268/BSGM2017v69n3a12

Ferrari, L., Tagami, T., Eguchi, M., Orozco-Esquivel, M. T., Petrone, C., Jacobo-Albarrán, J., & López-Martínez, M. (2005). Geology, geochronology and tectonic setting of late Cenozoic volcanism along the southwestern Gulf of Mexico: the Eastern Alkaline Province revisited. *Journal of Volcanology and Geothermal Research,* 146(4), 284–306. https://doi.org/10.1016/j.jvolgeores.2005.02.004

Fitz-Díaz, E., Lawton, T. F., Juárez-Arriaga, E., & Chávez-Cabello, G. (2018). The Cretaceous-Paleogene Mexican orogen: Structure, basin development, magmatism and tectonics. In A. Gómez-Tuena, F. Ortega-Gutiérrez (Eds.), Tectonic Systems of Mexico: Origin and Evolution. *Earth-Science Reviews, 183*, 56–84. https://doi.org/10.1016/j.earscirev.2017.03.002

Furre, A. K., Eiken, O., Alnes, H., Vevatne, J. N., & Kiær, A. F. (2017). 20 years of monitoring CO_2-injection at Sleipner. *Energy Procedia*, *114*, 3916–3926.

Guzmán-Arellano, G. J. (2012). *Evaluación petrolera y método de explotación de la región Tampico Misantla* [Bachelor Thesis]. Facultad de Ingeniería, Universidad Nacional Autónoma de México.

Hamblock, J. M. (2002). *Lithology, mineralization and alteration in the Eastern Alkaline Province* [M. Sc. Thesis]. Universidad de Arizona.

Hatzignatiou, D. G., Riis, F., Berenblyum, R., Hladik, V., Lajka, R., & Francu, J. (2011). Screening and evaluation of a saline aquifer for CO_2 storage: Central Bohemian Basin, Czech Republic. *International Journal of Greenhouse gas Control,* 5, 1429-1442. https://doi.org/10.1016/j.ijggc.2011.07.013

IEA-GHG (2009). *Development of storage coefficients for CO_2 storage in deep saline formations* (Technical study report 2009/13). IEA Greenhouse Gas R&D Programme, Vienna.

Lawton, T. F., Juárez-Arriaga, E., Ocampo-Díaz, Y. Z. E., Beltrán-Triviño, A., Martens, U., & Stockli, D. (2016). Evolution of late Cretaceous-Paleogene foreland sediment-dispersal systems of Northern and Central Mexico. *35th Annual GCSSEPM, Fundation Perkins-Rosen Research Conference Programs and Abstracts*, *Houston, Texas*, 216–233.

López-Doncel, J. (2003). La Formación Tamabra del Cretácico medio en la porción central del margen occidental de la Plataforma Valles-San Luis Potosí, centro-noreste de México. *Revista Mexicana de Ciencias Geológicas*, *20*(1), 1–19.

Luo, A., Yongming, L., Chen, X., Zhu, Z., & Peng, Y. (2022). Review of CO_2 sequestration mechanism in saline aquifers. *Natural Gas Industry*, *9*, 383–393. https://doi.org/10.1016/j.ngib.2022.07.002

Martini, M., & Ortega, F. (2018). Tectono-stratigraphic evolution of eastern Mexico during the break-up of Pangea: A review. *Earth-Science Reviews, 183*, 38–55. DOI: 10.1016/j.earscirev.2016.06.013

Matthews, W. R., & Kelly J. (1967). How to predict formation pressure and fracture gradiente. *Oil and Gas Journal*, *65*, 92–1066.

Medina, E., Levresse, G., Carrera, J., & Cerca, M. (2023). A basin scale assessment framework of onshore aquifer-based CO_2 suitability storage in Tampico Misantla basin, Mexico. *International Journal of Greenhouse Gas Control*, *125*, 103874, DOI: https://doi.org/10.1016/j.ijggc.2023.103874

Nava-Perez, M., & Alegria-Luna, M. A. (2001). *Los sistemas petroleros de la región de Tampico-Misantla* [Bachelor Thesis]. Facultad de Ingenería, Universidad Nacional Autónoma de México.

Poliquin, M. J. (2009). *Geology, Geochemistry and age of intrusion-related mineralisation in eastern Mexico* [Ph. D. Thesis]. Exter University.

Pindell, J., Villagómez, D., Molina-Garza, R., Graham, R., & Weber, B. (2020). A revised synthesis of the rift and drift history of the Gulf of Mexico and surrounding regions in the light of improved age dating of the Middle Jurassic salt. *Geological Society, London, Special Publications*, *504*, 29–76. https://doi.org/10.1144/SP504-2020-43

Rodríguez–Hernández, E., Lopez Doncel, R., Barboza Gudiño, J. R., & Cruz Marquez, J. (2007). Análisis sedimentológico-facial de clastos formadores de brechas calcáreas cretácicas de una zona transicional plataforma–cuenca en el centro de México. *Revista Mexicana de Ciencias Geologicas,* 26, 687–708.

Roure, F., Alzaga-Ruiz, H., Callot, J. P., Ferket, H., Granjeon, D., Gonzalez-Mercado, G. E., Guilhaumou, N., Lopez, M., Mougin, P., Ortuno-Arzate, S., & Séranne, M. (2009). Long lasting interactions between tectonic loading, unroofing, post-rift thermal subsidence and sedimentary transfers along the western margin of the Gulf of Mexico: Some insights from integrated quantitative studies. *Tectonophysics*, *475*(1), 169–189. https://doi.org/10.1016/j.tecto.2009.04.012

Segerstrom, K. (1962). Geology of South-central Hidalgo and Northeastern México, Mexico. *United States Geological Survey Bulletin*, 1104-C, 87–162.

Seibertz, E. (1986). Paleogeography of the San Felipe Formation (Mid-Cretaceous, NE Mexico) and facial effects upon inoceramids of the Turonian/Coniacian transition. *Zentralblatt für Geologie und Paläontologie*, *I*(9/10), 1171–118. DOI: 10.1127/zbl_geol_pal_1/1985/1986/1171

Servicio Geológico Mexicano (1997a). Carta geológica-minera Cuidad Valle, F14-8, 1:250 000.

Servicio Geológico Mexicano (1997b). Carta geológica-minera Pachuca, F14-11, 1:250 000.

Servicio Geológico Mexicano (1999). Carta geológica-minera Cuidad Mande, F14-5, 1:250 000.

Servicio Geológico Mexicano (2002). Carta geológica-minera Veracruz, E14-3, 1:250 000.

Servicio Geológico Mexicano (2004a). Carta geológica-minera Cuidad Victoria, F14-2, 1:250 000.

Servicio Geológico Mexicano (2004b). Carta geológica-minera Poza Rica, F14-12, 1:250 000.

Servicio Geológico Mexicano (2004c). Carta geológica-minera Tampico, F14-3-6, 1:250 000.

Servicio Geológico Mexicano (2004d). Carta geológica-minera Tamiahua, F14-9, 1:250 000.

Suter, M. (1980). Tectonics of the external part of the Sierra Madre Oriental foreland thrust-and-fold belt between Xilitla and the Moctezuma River (Hidalgo and San Luis Potosi states). *Revista del Instituto de Geología, Universidad Nacional Autónoma de Mexico*, *4*, 19–31.

Todd, R. G. (1976). Oolite-Bar Progradation, San Andres Formation, Midland Basin, Texas. *AAPG Bulletin, 60*(6), 907–925. https://doi.org/10.1306/C1EA35DC-16C9-11D7-8645000102C1865D

Torp, T. A., & Gale J. (2003). Demostrating storage of CO_2 in geological reservoirs, the Sleipner and SACS projects. *Proceedings of the 6th International Conference on Greenhouse Gas Control Technologies. Kypto. Japón*, V1- 311–316.

U.S. DOE, (2007). *Final Report 2007 Strategic Center for Coal Carbon Sequestration Peer Review Meeting. Pittsburgh, Pennsylvania September, 17–20.* U.S. Department of Energy, National Energy Technology Laboratory.

Viera-Décida, F., Ramirez Fernandez, J. A., Velasco Tapia, F., & Orozco Esquivel, M. T. (2009). Relaciones petrogenéticas del magmatismo en la provincia Alcalina Oriental mexicana. *Ciencias UANL*, *12*(1), 42–49.

Weijmars, R. (2024). Concurrent challenges in practical operations and modeling of geological carbon-dioxide sequestration: Review of the Gorgon project and FluidFlower benchmark study. *Energy Strategy Reviews*, 101586.

White., D. J. (2011). Geophysical monitoring of the Weyburn CO_2 flood: Results during 10 years of injection. Energy Procedia, 4, 3628-3635.

Wyllie, M. R. J., & Rose, W. D. (1950). Some Theoretical Considerations Related to the Quantitative Evaluation of the Physical Characteristics of Reservoir Rock from Electric Log Data. *Transaction of American Institute of Mining Engineers,* 189, 105–118.

Zhou, Q., Bitkholzer, J. T., Tsang, C. F., & Rutqvist, J. (2008). A method for quick assessment of CO_2 storage capacity in closed and semi-closed saline formations. *International Journal of Greenhouse Gas Control*, *2*, 626–639.

Zimmerman, R. W. (1991). *Compressibility of sandstones. Development in Petroleum Science*. Elsevier Science Publishers, vol. 29.